Photocatalytic degradation of antibiotic enrofloxacin under solar light using ZnO and Bi_2MoO_6 materials

Qinzheng Wei[1], *Sze-Mun* Lam[2], *Haixiang* Li[1*] and *Jin-Chung* Sin[2]

[1]Guilin University of Technology, Guilin 541004, China
[2]Universiti Tunku Abdul Rahman, Jalan Universiti, 31900 Kampar, Perak, Malaysia

Abstract: Enrofloxacin (ENR) as one of the most commonly used veterinary antibiotic in the aquaculture industry has led to serious water pollution due to its extensive use. In this study, ZnO catalysts were synthesized using a facile precipitation method, while the Bi_2MoO_6 catalysts were prepared via a solvothermal method. The resulting materials underwent comprehensive characterization using techniques such as scanning electron microscopy (SEM), energy-dispersive X-ray spectroscopy (EDS), X-ray diffraction (XRD), Fourier transform infrared spectroscopy (FTIR), ultraviolet-visible diffuse reflectance spectroscopy (UV-vis DRS), and photoluminescence spectroscopy (PL) to investigate their physical, chemical, and optical properties. Subsequently, the devised catalysts were scrutinized for degradation of ENR under simulated solar light irradiation. The degradation efficiency of ENR by Bi_2MoO_6 nanosheets reached 69.08%, which greatly exceeded that of ZnO 38.30%.

1 Introduction

In recent years, the aquaculture industry has witnessed rapid development.To safeguard aquatic products against bacteria, farmers routinely employed substantial quantities of veterinary antibiotics, including the fluoroquinolone antibiotic ENR during the feeding process. Unfortunately, the resulting wastewater is often discharged into the environment without undergoing complete metabolic transformation in the animal's body, leading to serious water pollution [1].Antibiotics as emerging contaminants possessed towering challenges for conventional treatment methods. However, advanced oxidation technologies such as photocatalysis have appeared as effective and environmentally friendly solutions. In particular, semiconductor photocatalysts have garnered considerable attention due to their capacities to directly harness solar energy for the degradation of a wide spectrum of organic pollutants, including and antibiotics, during wastewater treatment [2, 3].

Among the diverse array of photocatalysts available today, zinc oxide (ZnO) stands out for its exceptional physical, chemical, and optical properties as well as its stability, and economic non-toxicity [4]. Similarly, bismuth molybdate (Bi_2MoO_6) has attracted significant interest owing to its unique structure and its ability to be activated by visible

*Corresponding author:lihaixiang0627@163.com

light [5]. The narrower bandgap of Bi_2MoO_6 extends the photoresponse range, facilitating the generation of photogenerated electron-hole pairs. This phenomenon serves as the foundation for subsequent redox reactions, ultimately leading to the degradation of target pollutants into water and carbon dioxide, with minimal or no production of toxic by-products [6].

In this study, the ZnO catalysts were synthesized by a facile precipitation method, while the Bi_2MoO_6 catalysts were prepared via a solvothermal method. The physical, chemical, and optical properties of these materials were systematically characterized. Furthermore, the photocatalytic performance of these photocatalysts were evaluated by evaluating the degradation of ENR under solar light irradiation for both species under identical conditions.

2 Materials and methods

2.1 Chemicals

All chemicals and reagents used in this study were of analytical purity and obtained directly from suppliers without further purification. Specifically, zinc acetate dihydrate ($C_4H_6O_4Zn{\cdot}2H_2O$) and formamide (CH_3NO) were procured from Sinopharm, while bismuth nitrate pentahydrate ($Bi(NO_3)_3{\cdot}5H_2O$) and sodium molybdate dihydrate ($Na_2MoO_4{\cdot}2H_2O$) were sourced from Aladdin. Ethylene glycol (EG), isopropanol (C_3H_8O), anhydrous ethanol (C_2H_5OH), and ammonia (H_5NO) were acquired from Xilong Science.

2.2 Synthesis of ZnO

The preparation of ZnO was based on the precipitation method as follows: 0.03 mol of zinc acetate dihydrate ($C_4H_6O_4Zn{\cdot}2H_2O$) was weighed and added into a beaker containing 150 mL of deionized water. Sequentially, 7.5 mL of ethylene glycol (EG) and 2.4 mL of formamide (CH_3NO) were poured into the resultant mixture. The solution pH was adjusted to 10 using ammonia , and the obtained solution was thoroughly stirred magnetically for 30 minutes. Subsequently, the solution was heated in an oven at 100°C for 30 minutes, resulting in the formation of a white precipitate. The precipitate was then washed with anhydrous ethanol and deionized water, followed by drying in an oven at 60°C for 12 hours to yield the white ZnO.

2.3 Synthesis of Bi_2MoO_6

The Bi_2MoO_6 were synthesized via a solvothermal method as follows: 2 mmol of bismuth nitrate pentahydrate ($Bi(NO_3)_3{\cdot}5H_2O$) and 1 mmol of sodium molybdate dihydrate ($Na_2MoO_4{\cdot}2H_2O$) were weighed and placed in two different beakers. Liquid A (containing bismuth nitrate) and liquid B (containing sodium molybdate) were obtained by magnetic stirring for 30 minutes. Liquid B was gradually added to liquid A, and 120 mL of isopropanol (C_3H_8O) was added in the mixture. After 30 minutes of constant stirring, a white solution formed. The mixture was transferred to a 200 mL PTFE-lined high-pressure reactor and treated in an oven at 160°C for 24 hours. Upon cooling to room temperature, the precipitates were washed with anhydrous ethanol and deionized water, followed by drying in an oven at 60°C for 12 hours to obtain the Bi_2MoO_6.

2.4 Characterization studies

Scanning electron microscope (SEM, HITACHI SU5000) was used to study the

micro-morphology of the materials, energy dispersive X-ray (EDS) to analyze the elemental composition and distribution of the materials, and X-ray diffractometer (XRD, X'Pert3 Power) to analyze the crystal structure of the synthesized samples. Functional group analysis was performed by FTIR spectrometer (FTIR, Thermo Fisher Scientific Nicolet iN10). UV-vis diffuse reflectance spectrometer (UV-vis DRS, Perkin Elmer Lambda 950) and photoluminescence spectroscopy (PL, Edinburgh FLS1000) were used to study the optical properties of the synthesized samples and the separation properties of the photogenerated charge carriers, respectively.

2.5 Photocatalytic experiments

The photoactivity of the synthesized products was systematically investigated through the solar light degradation efficiency of ENR. The photocatalyst was dosed at a concentration of 0.5 g/L, while the antibiotic ENR was maintained at a concentration of 5 mg/L. The dark reaction is carried out first, during which the solution underwent absorption-desorption equilibrium for 30 minutes under dark conditions. Subsequently, the photocatalytic process was initiated by irradiating the mixture using a 500 W xenon lamp to simulate solar light. Following this, 5 mL of the ENR solution was collected, and its initial concentration (C_0) was quantified at 271 nm using a UV spectrophotometer. The reaction was then allowed to proceed with the remaining solution, and additional 5 mL samples were collected at 30-minute intervals to measure their concentrations (C).

3 Results and discussion

3.1 Morphology and elemental analyses

The morphological structure of each sample was observed by scanning electron microscopy (SEM). Figure 1a shows the as-prepared ZnO sample, which consisted of tightly connected octagonal prisms in the length ranges of 1-5 μm with relatively flat and smooth surfaces. Figure 1b shows the as-prepared Bi_2MoO_6 sample, which consisted of nanosheets with a particle size of about 50-100 nm. Moreover, compared to the 1-5 μm size of ZnO,Bi_2MoO_6 had a smaller nanosheet morphology with particle size of approximately 50-100 nm and aggregated or overlapped to form a monolith.

EDS elemental mapping analyses were utilized to validate the elemental composition of the synthesized ZnO sample and their spatial distributions. The EDS mapping images distinctly revealed the homogeneous distribution of Zn and O elements in the ZnO sample as illustrated in Figure 1c. Similarly, in Figure 1d，Bi,Mo and O elements were evenly distributed in the Bi_2MoO_6 sample.

3.2 Crystal phase analysis

The crystal structure and phase composition of the synthesized samples were utilized to examine using X-ray diffraction (XRD). The XRD data for the samples are displayed in Figure 2a. The XRD data for the samples are presented in Figure 2a. For the ZnO nanoprisms, all the characteristic diffraction peaks were well aligned with the hexagonal wurtzite ZnO (JCPDS No.36-1451) [7]. On the other hand, the observed diffraction peaks at 2θ values of 28.31°, 32.53°, 46.74°, 55.44°, and 58.48° were corresponded to the crystallographic planes (131), (200), (202), (331), and (262), respectively, for the pure Bi_2MoO_6 nanosheets. These findings were consistent with the crystallographic planes of rhombohedral Bi_2MoO_6 (JCPDS No.21-0102) [8]. Notably, no other peaks were detected,

and the presence of sharp and narrow diffraction peaks confirmed the high purity of the synthesized materials.

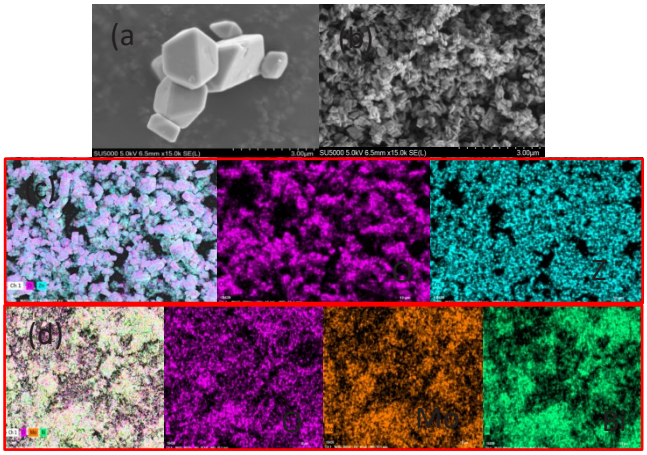

Fig. 1. SEM images of (a) ZnO nanoprisms and, (b) Bi_2MoO_6 nanosheets and; EDS mapping images of (c) ZnO nanoprisms and, (d) Bi_2MoO_6 nanosheets.

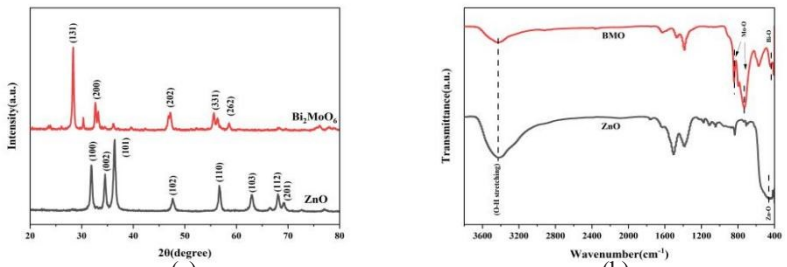

Fig. 2. (a) XRD patterns of ZnO sample and Bi_2MoO_6 sample and;(b) FTIR profiles of ZnO sample and Bi_2MoO_6 sample.

3.3 Functional group analysis

The FTIR analysis technique was used to investigate the functional group composition of the samples. The FTIR spectra of the as-synthesized ZnO and Bi_2MoO_6 materials were recorded in the wavenumber range of 400 cm^{-1} to 4000 cm^{-1}, as depicted in Figure 2b. In the FTIR spectra of Bi_2MoO_6, the peak at 443 cm^{-1} was attributed to Bi-O stretching and bending vibrations [9].The prominent peaks at 726 cm^{-1} and 843 cm^{-1} in the Bi_2MoO_6 was spectra corresponded to Mo-O stretching vibration [10].In the FTIR spectra of ZnO, the absorption peak observed at 449 cm^{-1} was attributed to the vibrational mode of Zn-O bond [11].Interestingly, the O-H hydrogen bond stretching vibration of water molecules was observed around 3438 cm^{-1} in the two catalysts. The -OH was an important functional group as it can produce the powerful hydroxyl radical to partake in the photocatalytic reaction.

3.4 Optical trait analysis

The UV-Vis DRS presented in Figure 3a were utilized to analyze the optical properties of

ZnO and Bi_2MoO_6. Notably, ZnO exhibited strong absorption in the UV region with an absorption limit at approximately 380 nm. In contrast, Bi_2MoO_6 displays strong absorption in the visible region (as shown in Figure 3a) with an absorption limit around 450 nm.

The band gap energy (Eg) of ZnO and Bi_2MoO_6 can be determined using the Kubelka-Munk formula [12]:

$$\alpha h\nu = A\ (h\nu - Eg)^{n/2} \quad (1)$$

where α, $h\nu$ and A are the absorption coefficient, discrete photon energy and constant, respectively. Also, n is decided by the transition type of the semiconductor sample(typically, n = 1 and n = 4 for direct transition and indirect transition, respectively.). Both ZnO and Bi_2MoO_6 are semiconductors of direct lepton type, so their n value was 1 [13]. Thus $\alpha h\nu$ was derived from the above equation and then the band gap energy was determined by the intercept of the $(\alpha h\nu)^2$ versus ($h\nu$) curve. Consequently, the band gap energies of ZnO and Bi_2MoO_6 were estimated to be 3.34 eV and 2.32 eV, respectively, as shown in Figure 3b.

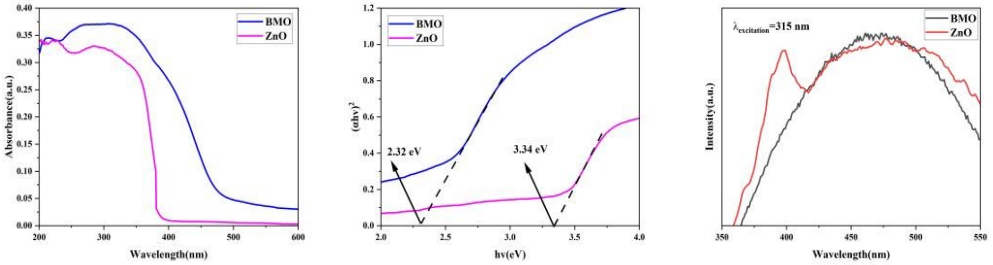

(a) (b) (c)

Fig. 3. (a) Uv-vis DRS of ZnO and Bi_2MoO_6; (b) band gap measurement of ZnO and Bi_2MoO_6 and;(c) Photoluminescence spectra of ZnO and Bi_2MoO_6 at 315 nm excitation wavelength.

3.5 Electronic property analysis

To explore these processes, photoluminescence spectroscopy (PL) was employed to investigate carrier migration and recombination in ZnO and Bi_2MoO_6. In general,PL spectra with weaker emission intensity indicated a lower rate of electron-hole pair recombination. Consequently, this expected to have higher photodegradation efficiency. Figure 3c displays the emission spectra of ZnO and Bi_2MoO_6 at an excitation wavelength of 315 nm, Bi_2MoO_6 had a strong emission peak at 470 nm. As shown in Figure 3c, Bi_2MoO_6 exhibited reduced PL intensity compared to ZnO, indicating enhanced charge carrier separation and improved photocatalytic efficiency.

3.6 Photocatalytic activity

The photocatalytic activity of ZnO and Bi_2MoO_6 materials was investigated for the photodegradation of ENR antibiotic under solar light. The characteristic maximum absorption wavelength (λ_{max}) of 271 nm was used for ENR.

Experimental conditions for both photocatalysts were identical, with a photocatalyst dosage of 0.5 g/L and an antibiotic pollutant concentration of 5 mg/L. Under solar light irradiation, the concentration of ENR decreased with increasing irradiation time (t) as shown in Figure 4a. Blank experiments demonstrated that the degradation of pollutants under solar light condition was minimal and negligible. The ZnO and Bi_2MoO_6 exhibited

similarly low degradation effect after 180 minutes of dark condition. This suggested that the ENR antibiotic was highly stable and required both a photocatalyst and light for effective degradation. After 180 minutes of irradiation, the degradation efficiencies of ZnO and Bi_2MoO_6 were 38.30% and 69.08%, respectively. Photodegradation efficiencies of ENR in presence of ZnO and Bi_2MoO_6 showed that Bi_2MoO_6 was more better result as compared to ZnO because of smaller particle size,nanosheet morphology and efficient separation and transfer of photogenerated electrons and holes.

The rate constant (k) of the applied catalyst was determined using the pseudo-first-order reaction kinetics $ln(C_0/C)=kt$, where C_0 and C represented the initial concentration at time interval t as shown in Figure 4b. The results indicated that the value of k for Bi_2MoO_6 (0.0065 min^{-1}) was approximately 2.41 times higher than that of ZnO (0.0027 min^{-1}). The obtained kinetic study findings were also consistent with the degradation efficiency.

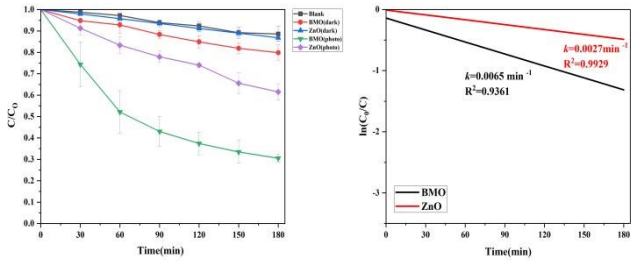

Fig. 4. (a) Plot of (C/C_0) versus time for degradation of ENR antibiotic under solar light irradiation and (b) Rate constants (k) corresponding to ZnO and Bi_2MoO_6.

4. Conclusion

In this study, ZnO nanoprisms were synthesized using the precipitation method, and followed by the preparation of Bi_2MoO_6 nanosheets via the solvothermal method. The high purity of the synthesized samples was confirmed through various characterization techniques.The photocatalytic degradation of the ENR antibiotic pollutant was investigated under solar light. The degradation efficiencies of Bi_2MoO_6 nanosheets reached 69.08%, which was significantly surpassing the 38.30% degradation efficiency observed for ZnO. The photodegradation reaction was modeled using pseudo-first-order kinetics, yielded a rate constant of 0.0065 min^{-1} for Bi_2MoO_6 nanosheets, which was 2.41 times higher than that of ZnO (0.0027 min^{-1}).The enhancement can be attributed to the smaller particle size and smaller bandgap of the Bi_2MoO_6 nanosheets, which extended the photoresponse range and enabled direct utilization of solar light. The generation of additional photogenerated electron-hole pairs further contributed to the improved efficiency of the photocatalytic degradation of the antibiotic ENR.

References

1. J. W. Peterson, B. H. Gu, M. D. Seymour, Surface interactions and degradation of a fluoroquinolone antibiotic in the dark in aqueous TiO_2 suspensions. J. Sci Total Environ. **532**, 398-403 (2015).http://dx.doi.org/10.1016/j.scitotenv.2015.06.024

2. R. Anjali, S. Shanthakumar, Insights on the current status of occurrence and removal of antibiotics in wastewater by advanced oxidation processes. J. J Environ Manag. **246**, 51-62 (2019). http://dx.doi.org/10.1016/j.jenvman.2019.05.090
3. A. Saravanan, V. C. Deivayanai, P. S. Kumar, et al., A detailed review on advanced oxidation process in treatment of wastewater: Mechanism, challenges and future outlook. J. Chemosphere. 308 (2022). http://dx.doi.org/10.1016/j.chemosphere.2022.136524
4. J. S. Packialakshmi, M. F. Albeshr, A. F. Alrefaei, et al., Development of ZnO/SnO_2/rGO hybrid nanocomposites for effective photocatalytic degradation of toxic dye pollutants from aquatic ecosystems. J. Environ Res. 225 (2023). http://dx.doi.org/10.1016/j.envres.2023.115602
5. T. Chankhanittha, V. Somaudon, J. Watcharakitti, et al., Performance of solvothermally grown Bi_2MoO_6 photocatalyst toward degradation of organic azo dyes and fluoroquinolone antibiotics. J. Mater Lett. 258 (2020). http://dx.doi.org/10.1016/j.matlet.2019.126764
6. G. Fan, S. Yang, B. Du, et al., Sono-photo hybrid process for the synergistic degradation of levofloxacin by $FeVO_4/BiVO_4$: Mechanisms and kinetics. J. Environ Res. 204 (2022). http://dx.doi.org/10.1016/j.envres.2021.112032
7. W. Xia, Y. Wang, Q. Wang, et al., Tubular acceptor-rich ZnO hierarchical heterostructure as an efficient photocatalyst for organic degradation. J. Appl Surf Sci. 506 **(**2020). http://dx.doi.org/10.1016/j.apsusc.2019.145008
8. Y. Tian, F. Zhou, S. Zhan, et al., Mechanisms on the enhanced sterilization performance of fluorocarbon resin composite coatings modified by $g\text{-}C_3N_4/Bi_2MoO_6$ under the visible-light. J. J Photochem Photobiol A-Chem. **350**, 10-6 (2018). http://dx.doi.org/10.1016/j.jphotochem.2017.09.043
9. R. Hejazi, A. R. Mahjoub, A. H. C. Khavar, et al., Novel visible-light-responsive rGO-ZnO@Bi_2MoO_6 nanocomposite with enhanced light harvesting and Z-scheme charge transfer for photodegradation and detoxification of RhB. J. Solid State Sci. 95 (2019). http://dx.doi.org/10.1016/j.solidstatesciences.2019.105934
10. J. Wang, C. Zhao, S. Yuan, et al., One-step fabrication of Cu-doped Bi_2MoO_6 microflower for enhancing performance in photocatalytic nitrogen fixation. J. J Colloid Interface Sci. **638**, 427-38 (2023). http://dx.doi.org/10.1016/j.jcis.2023.02.005
11. L. Zhang, L. Zhang, Y. Chen, et al., CdS/ZnO: A Multipronged Approach for Efficient Reduction of Carbon Dioxide under Visible Light Irradiation. J. ACS Sustain Chem Eng. **8(13)**, 5270-7 (2020). http://dx.doi.org/10.1021/acssuschemeng.0c00190
12. M. Ghorbani, M. Frahadian, M. Khosravi, et al., Facile synthesis of Z-scheme ZnO-nanorod @ BiOBr-nanosheet heterojunction as efficient visible-light responsive photocatalyst: The effect of electrolyte and scavengers. J. J Photochem Photobiol A-Chem. 429 (2022). http://dx.doi.org/10.1016/j.jphotochem.2022.113930
13. D. Xu, F. Sun, H. Shao, et al., Bi_2MoO_6 nanosheets assembled on $LaFeO_3$ nanofibers with n-p type hierarchical nanostructure for enhanced HCHO sensor. J. Sens Actuator B-Chem. 406 (2024). http://dx.doi.org/10.1016/j.snb.2024.135430